Article

pubs.acs.org/Biomac

Silk Reconstitution Disrupts Fibroin Self-Assembly

Sean R. Koebley,[†] Daniel Thorpe,[†] Pei Pang,[†] Panos Chrisochoides,[†] Imke Greving,[‡,§] Fritz Vollrath,[‡] and Hannes C. Schniepp*[,†]

[†]The College of William & Mary, Department of Applied Science, P.O. Box 8795, Williamsburg, Virginia 23187-8795, United States

[‡]Oxford Silk Group, Department of Zoology, Oxford University, Tinbergen Building, South Parks Road, Oxford, Oxfordshire OX1 3PS, United Kingdom

Supporting Information

ABSTRACT: Using atomic force microscopy, we present the first molecular-scale comparison of two of the most important silk dopes, native (NSF) and reconstituted (RSF) silkworm fibroin. We found that both systems depended on shear to show self-assembly. Significant differences in the nature of self-assembly between NSF and RSF were shown. In the highest studied concentration of 1000 mg/L, NSF exhibited assembly into 20−30 nm-wide nanofibrils closely resembling the surface structures found in natural silk fibers. RSF, in contrast, showed no self-assembly whatsoever at the same concentration, which suggests that the reconstitution process significantly disrupts silk's inherent self-assembly capability. At lower concentrations, both RSF and NSF formed fibrils under shear, apparently denatured by the substrate. Using image analysis, we quantified the properties of these self-assembled fibrils as a function of concentration and found low-concentration fibrils of NSF to form larger continuous structures than those of RSF, further supporting NSF's superior self-assembly capabilities.

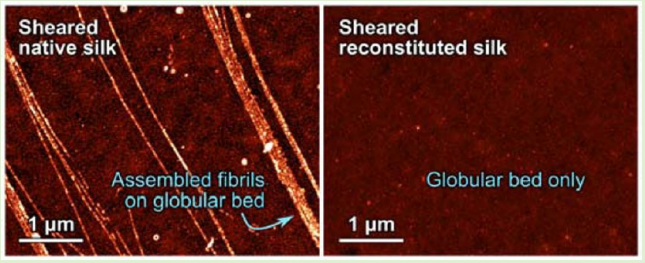

INTRODUCTION

Silk has promise as a next-generation engineering and biomedical material. A natural polymer, silk is spun by spiders and insects at ambient temperature and pressure to form a biocompatible, biodegradable fiber of exceptional toughness.[1,2] Yet despite the increased development of silk-based devices with interesting (and potentially important) bioengineering and medical applications,[3−5] the mechanical properties of silk-derived "artificial" fibers and films remain inferior to those of their natural prototypes.[6] Silk structure determines its function, hence our current inability to mimic the intricate spinning process and hierarchical structure of natural silk limits the performance of artificially made silks.[1,7] Further investigation of silk assembly and structure is needed in order to improve the properties of artificial silks and synthesize their molecules effectively, be it *de novo* or from reconstituted silk fibroin (RSF).[8,9] Here, we compared the morphological differences of molecular-scale self-assembly of two of the most important silk dopes in order to further our understanding: native silk fibroin (NSF) and RSF, which are both produced by the silkworm *Bombyx mori*.

The natural spinning of silk is a sophisticated process that, for both insects and spiders, involves an internal draw-down, pH drop, exchange of ions, and removal of water to yield a tough, water-insoluble fiber from aqueous dope.[10] In the case of the silk spun by the domesticated silkworm, *Bombyx mori*, the dope primarily consists of the 350 kDa heavy-chain, 25 kDa light-chain, and 30 kDa P25 silk proteins (fibroins).[11] *Bombyx* fibroin is composed of hydrophobic and hydrophilic blocks, which induces micellular folding in an aqueous environment.[12−14] Together, the three fibroins—collectively referred to as NSF—form a 6:6:1 complex of heavy-chain, light-chain, and P25, respectively, when stored at high concentration (20−30 wt %) in the silkworm's middle storage gland.[11,15] Just prior to entering the anterior spinning duct, the silk dope is in a liquid crystalline state[10,16] with a characteristic secondary structure (Silk I) distinguished by a type-II β-turn signature.[17,18] As the dope moves through the exponentially decaying diameter of the silkworm's duct, the forces of flow elongation, tensile pulling and possibly also shear experienced at the duct walls further align the fibroin molecules, causing shear thinning and expulsion of water from the dope.[10,19,20] Once extruded from the silkworm's spigot, the resulting fiber is water-insoluble and readily characterized by its antiparallel β-sheet structure (Silk II).[17,21] Shear and water loss are regarded as the key factors in silkworm silk assembly:[10,19,22] their combination is suggested to cause the hydrophobic regions of the fibroin molecules to interact and form β-sheets,[12,23] and near-native structure and fibrillar morphology has been achieved through shear force alone.[24,25] While shear is known to be crucial, the precise details of how it transforms fibroin molecules into the fibrillar, hierarchical morphology observed in natively spun fibers remain elusive.[26]

Received: May 31, 2015
Revised: July 15, 2015
Published: August 18, 2015

DOI: 10.1021/acs.biomac.5b00732
Biomacromolecules 2015, 16, 2796−2804

In this study, we were particularly interested in the behavior of fibroin produced via reconstitution of silkworm cocoons. Typically, this RSF is synthesized by first boiling away the proteinacious sericin that coats the silken cocoon, dissolving the degummed silk in a chaotropic salt like LiBr or an ionic liquid, and dialyzing the resulting aqueous solution to remove the salt.[27] Cocoons are harvested in massive quantities for commercial textile production and can be stored for months.[28] Moreover, the reconstitution process can be instituted in bulk, which makes RSF an affordable, convenient, and thus very popular source of fibroin: a major fraction of all silk studies and the majority of all silk applications and devices use RSF as their source of silk.[8] There is mounting evidence, however, that the reconstitution process disrupts the native structure and bonding character of the fibroin molecule,[6,26,29,30] which motivated us to study whether the self-assembly behavior of fibroin is retained after the reconstitution process.

The experimental investigation of silk assembly is challenging; a variety of analytical techniques have been employed for in vitro studies. NMR,[17,18,31] X-ray scattering,[21,32] and other techniques[26,33] have been vital in discerning fibroin's secondary structure transition, while rheology has provided quantitative assessment of the influence of shear on silk's viscoelastic properties.[20,26] For a detailed view of the morphology of assembled silk structures, however, bulk techniques prove inadequate. Optical and electron microscopy have contributed valuable morphological insight,[25,34] but optical microscopy cannot resolve molecular-scale features, and electron microscopy necessitates dehydration and metallic coating of the sample. On the other hand, the imaging technique used in this study, atomic force microscopy (AFM), is capable of yielding 3D morphology of a protein sample with nanometer resolutions in the absence of harsh treatment or forces.[35] AFM has been employed to image silk and other biomolecules with unprecedented resolutions, providing valuable confirmation of existing theories and novel insight into assembly and other processes.[34−37]

In this work, we employed AFM imaging to directly compare the molecular-scale morphologies of RSF and NSF for the first time. In particular, we were interested in the intermolecular assembly of fibroin in response to shear and rapid water loss, which are likely to be the most important elements of in vivo assembly.[10,19,22] This is in contrast to previous studies, which have used heat,[34,38] cyclic concentration and dilution,[34,39−41] slow-drying,[42,43] alcohol,[8] pH,[44,45] flow in a rheometer,[25,26] or electrospinning[39,43]—mostly unnatural conditions—to facilitate silk assembly. We simply spin-coated a droplet of aqueous silkworm fibroin onto a substrate, which effectively applied the desired shear and rapid dehydration.[46] We previously described the result of spin-coating NSF:[24] the fibroin spontaneously formed straight nanofibrils, hundreds of micrometers long and often bundled, resembling the fibrillar meso-structure observed on the surface of naturally spun silkworm and spider silk fibers.[47−49] In this study, we applied shear to RSF as well as NSF via spin-coating and then visualized the obtained structures with molecular-resolution noncontact AFM. Comparison between these two essential fibroin dopes is important, especially regarding the viability of the widely used RSF as a fully functional silk source.

EXPERIMENT (MATERIALS AND METHODS)

Sample Preparation. RSF was prepared by first degumming *Bombyx mori* silk cocoons (Aurora Silks) to remove the sericin coating by heating at 70 °C in 0.5 wt % Na_2CO_3 for 3 h. After drying overnight, the silk was then stirred in a solution of 9 M LiBr at 70 °C until dissolved (about 30 min). A ratio of 2 g silk: 10 mL 9 M LiBr was preserved in each sample in order to preserve the consistency of the RSF molecular weight.[29] To extract the protein, we dialyzed the dissolved silk in 12000−14000 MWCO cassettes (Medicell International) against an excess of Millipore water (Millipore Synergy UV) for 48 h, changing the water twice. A silver nitrate test confirmed that no significant amount of LiBr was present in solution following dialysis. The concentration of the resulting RSF was determined by weighing an aliquot before and after heating in a vacuum oven at 70 °C for 30 min.

NSF was extracted directly from the middle storage glands of mature *Bombyx mori* silkworms. The silkworms were raised on a diet of mulberry leaves until their fifth instar, when their silk glands were dissected, with care taken to avoid shearing the silk dope. The extracted silk protein was gently washed in Millipore water to remove the sericin coating, then left overnight at 4 °C in Millipore water.

To prepare AFM samples, serial dilutions in Millipore water were first performed on each stock solution to achieve the desired concentrations. Five microliter drops of each concentration were placed on cleaved, atomically smooth mica substrates and either exposed to shear or allowed to deposit without shear. Only fresh solution (<1 h of incubation) was employed to create the samples. For shear-free conditions, the RSF solution was allowed to rest on mica at ambient temperature and humidity (20−25 °C, 20−50% relative humidity) for 5 min to promote the deposition of RSF proteins without significant evaporation. The nonsheared sample was then gently rinsed with Millipore water to remove the excess solution and dried with N_2 gas (Nitrogen 5.0, GTS Welco), with low flows of rinse and N_2 gas employed to avoid shearing the sample. To induce a radial shear field, the mica substrate was spin-coated for 3 min at 2000 rpm using a WS-650SZ Spin Processor (Laurell Technologies Corporation).

Atomic Force Microscopy. Samples were imaged with an NTEGRA Prima Scanning Probe Laboratory (NT-MDT) atomic force microscope at ambient conditions in sample scanning mode, using the Universal Head (SF005NTF, NT-MDT) and a 100 μm × 100 μm × 10 μm closed-loop piezo scanner (SC100NTF, NT-MDT). We used AppNano ACTA 200 silicon AFM probes (APPNANO), with a tip radius <10 nm, a resonant frequency of ≈300 kHz, and a nominal spring constant of 25−75 N/m. Noncontact AFM imaging conditions (the presence of net attractive forces) were confirmed by observation of a positive phase shift with respect to the free cantilever oscillation,[50] which we found at ≈80% of the free amplitude. To facilitate direct quantitative comparison between our AFM images, consistent values for scanning range (5 μm × 5 μm), resolution (1024 pixels ×1024 pixels), and scanning speed (0.7 Hz) were employed in most cases.

Image Analysis. NOVA Image Analysis (NT-MDT) and Gwyddion (http://gwyddion.net) were used to process our AFM scans. Cross sections of fibril height and width were made using NOVA Image Analysis. A sample size of n = 40 was utilized for all but the 1000 mg/L concentration NSF scans, where sample sizes of n = 26 reflected the lower number of visible unique fibrils. In order to assess width and height of the fibrils, full width at half-maximum, and height of the cross sections were calculated and analyzed using MATLAB. Volumes of individual globules and silk fibrils were calculated using a rotated-solid model (see Supporting Information).

Quantitative analysis of the fibril network was performed using Fiji/ImageJ (http://fiji.sc/Fiji) and MATLAB (Mathworks, Inc.). Therefore, a topography threshold was first applied to the AFM images in order to establish a binary distinction between particles/fibers and the substrate background. The Analyze Particles routine in ImageJ was then employed to determine the area and number of continuous fibroin particles/assemblies. To compensate for differences in tip size and scanning parameters between different experiments, a correction factor was used (see Supporting Information). Additionally, a minimum cutoff in particle area was imposed to keep individual outlier pixels from artificially distorting the particle size distribution

DOI: 10.1021/acs.biomac.5b00732
Biomacromolecules 2015, 16, 2796−2804

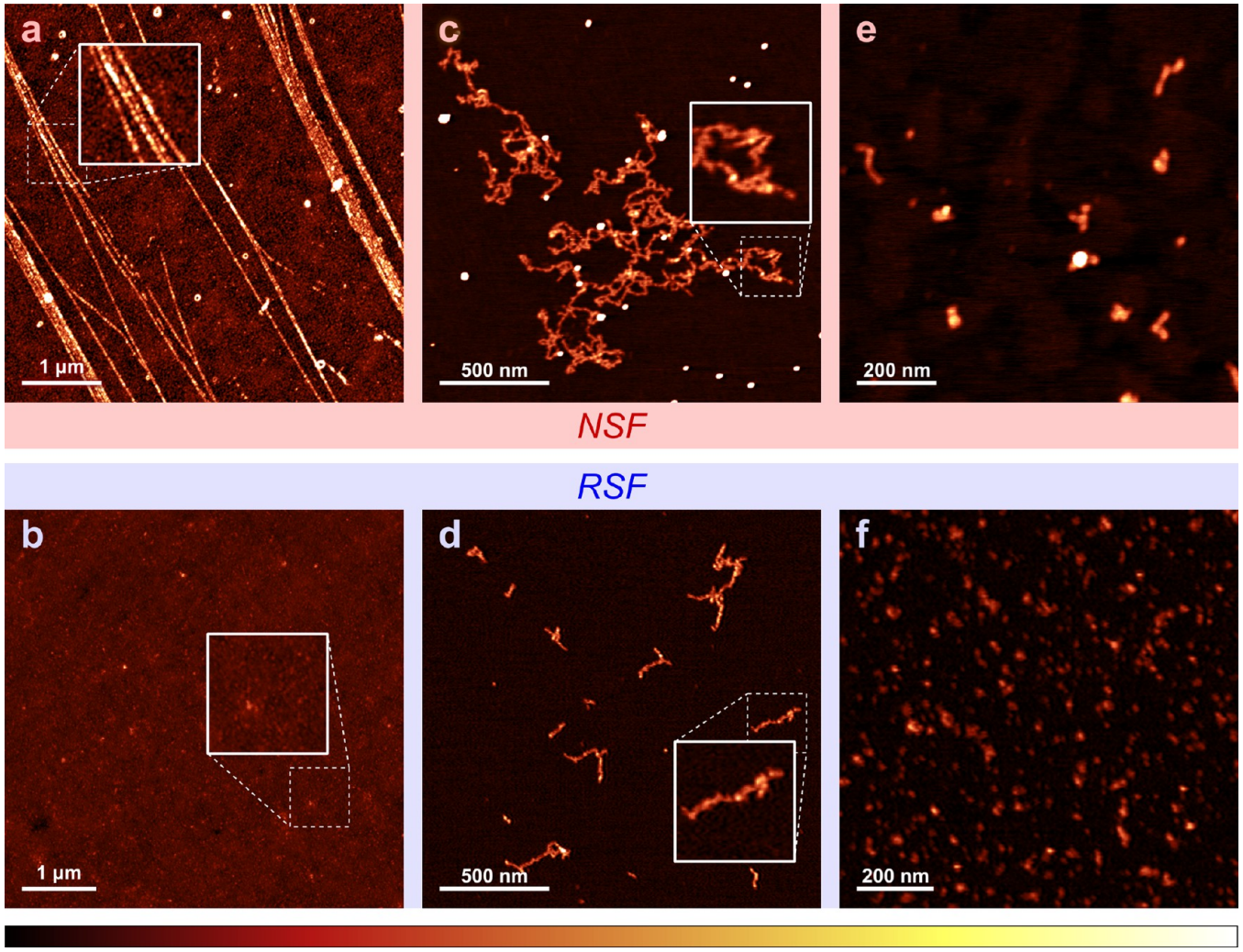

Figure 1. Noncontact AFM scans revealing the morphology of native silk fibroin (NSF, top row, red frame) and reconstituted silk fibroin (RSF, bottom row, blue frame). Under shear, 1000 mg/L NSF formed long, straight fibrils atop a bed of globular protein (a), while sheared 1000 mg/L RSF produced only globules (b). Shearing 10 mg/L dope resulted in long, coiled NSF fibrils (c) and short, branched RSF fibrils (d). Nonsheared samples at lower concentrations displayed a globular protein morphology: 10 mg/L NSF (e) and 100 mg/L RSF (f). Color bar: 7.5 nm for panels (a) and (b); 2 nm for panels (c)–(f).

(see Supporting Information). In order to analyze the branch length of the fibril network, a separate image analysis procedure was used. The binary topography images were skeletonized using the Skeletonize and AnalyzeSkeleton plugins; Skeletonize iteratively and symmetrically erodes particles outlined in a binary image until only a single, characteristic string of pixels remains.[51] Prior to skeletonization, a 2 nm Gaussian blur was applied to each topography-thresholded image in order to smooth the effects of thresholding and reduce spurious branching, and a minimum cutoff set at the width of a single fibril was also imposed to prevent fibril nodes, point topographies, and other irregularities from being counted as fibrils (see Supporting Information). The AnalyzeSkeleton plugin returned the length of each fibril and the number of fibrils. To average over sample inhomogeneities, multiple scans from different areas of the each sample were tested. The resulting fibril length distributions were similar enough that a rigorous statistical analysis presented strong evidence that they were sampled from the same population (Kruskal–Wallis Test, see Supporting Information).

RESULTS

Comparison of Natural Silk Fibroin and Reconstituted Silk Fibroin Assembly. In order to compare the molecular-scale behavior of NSF and RSF under shear, we first spin-coated dope samples onto mica. Prepared at a concentration of 1000 mg/L, NSF formed long, straight fibrils atop a bed of globular protein (Figure 1a), as previously described.[24] These nanofibrils exhibited the typical "beads-on-a-string" morphology,[24] reaching an apparent height[52] of 3.4 ± 0.5 nm and width of 27 ± 4 nm. The very same experiment with RSF, also at a concentration of 1000 mg/L, revealed that RSF failed to show any assembly into fibrils or any other discernible morphology (Figure 1b); instead, we only observed a uniform, globular bed of protein. This experiment already demonstrates that the self-assembly of RSF is substantially different from NSF: while NSF assembles into nanofibrils atop an underlying distribution of globules when exposed to shear via spin-coating, RSF forms only the globular bed.

Molecular self-assembly under shear was also observed when even lower concentrations were studied. Spin-coating 10 mg/L NSF dope yielded long, coiled nanofibrils of apparent height and width of 0.8 ± 0.1 nm and 13 ± 3 nm, respectively (Figure 1c), matching previous observations.[24] However, these fibrils are distinctly different from the 3.4 nm-high, 27 nm-wide, straight, beaded fibrils formed at higher concentrations (Figure

DOI: 10.1021/acs.biomac.5b00732
Biomacromolecules 2015, 16, 2796–2804

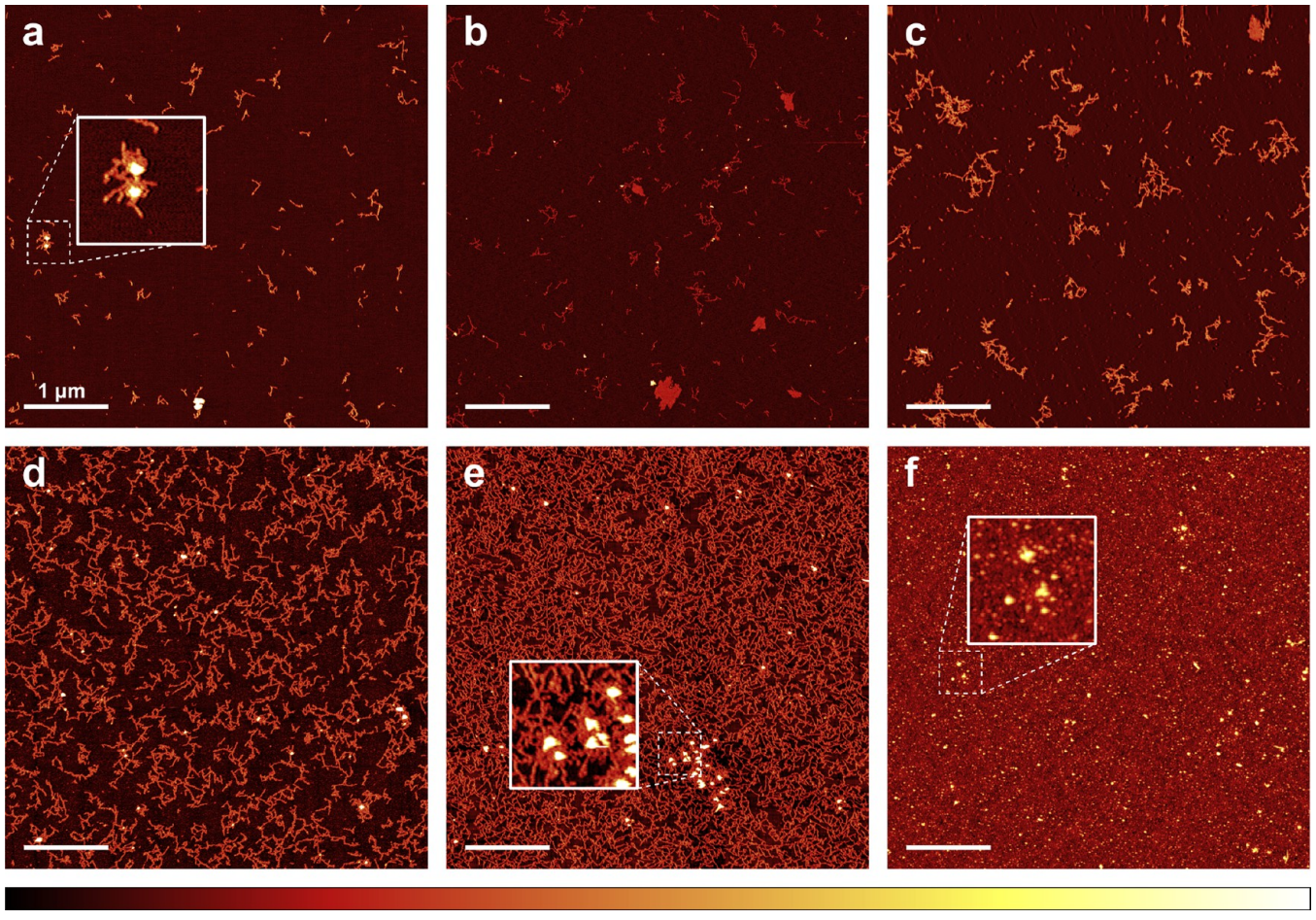

Figure 2. Shear-induced assembly of RSF at concentrations of 10 mg/L (a), 20 mg/L (b), 50 mg/L (c), 100 mg/L (d), 200 mg/L (e), and 500 mg/L (f). The 500 mg/L sample displayed a globular structure ((f) inset), while all other concentrations showed RSF assembling into short, branched fibrils (a, inset). The a, e, and f insets feature multilayer globular aggregates observed at all concentrations. Scale bars: 1 μm. Color bar: 3 nm for panels a–e, 7 nm for panel f.

1a). In contrast, the low-concentration fibrils displayed a more irregular morphology: interspersed globules, rod-like junctions, and other disordered components appear to form the fibril substructure (inset, Figure 1c). Interestingly, the RSF, which did not show any tendency of shear-induced assembly at the higher concentration of 1000 mg/L (Figure 1b), did exhibit assembly into nanofibrils when sheared at the lower concentration of 10 mg/L (Figure 1d). Compared to NSF, the RSF nanofibrils appear shorter and more branched, with slightly greater height (1.0 ± 0.2 nm) and nearly equivalent width (13 ± 2 nm). Similar self-assembling morphology of RSF has been reported in the literature, except that assembly was triggered by treatments other than shear in these cases, e.g., slow-concentrating, drying with compressed air, heating, or alcohol treatment.[34,36,37,42,53−55] The size of the fibrils rules out the possibility that they are individual, denatured proteins, as their volumes (>1000 nm^3) are far greater than the 180−450 nm^3 volume of a single NSF molecule.[37,53] We note that the lateral dimensions of the imaged protein structures are of the same order as the size of the AFM probes used, and consequently, the apparent widths are most likely overestimated and heights underestimated relative to their true values.[52,56] Therefore, precise determinations of dimensions and volumes are very challenging. Nevertheless, relative comparisons to other AFM data, as well as coarse general assessments are feasible and useful.

In order to determine the role of shear in the molecular self-assembly of NSF and RSF fibroin, nonsheared low-concentration NSF (10 mg/L) and RSF (100 mg/L) samples were studied (Figures 1e,f). In both cases, the evidence suggests the presence of individual fibroin molecules with a globular morphology, which aggregated into small clusters in many cases. However, many globules were isolated enough to allow us to estimate their dimensions: 15 ± 4 nm in width and 1.0 ± 0.2 nm in height for NSF;13 ± 3 nm in width and 0.6 ± 0.1 nm in height for RSF. The calculated volumes of the globules fell into the range 100−350 nm^3, which is in agreement with previous volume calculations of an individual fibroin molecule (180−450 nm^3).[37,53] Assigning a globular morphology to an individual silk protein is also in agreement with previously published AFM data of nonsheared fibroin[24,40,57] and computational assessments of native fibroin conformation based on scattering results.[32,40] Even at higher concentrations (1000 mg/L), scans showed only globules on the surface, albeit completely covering the surface (Figure S1). It is notable that for both RSF and NSF, shear was necessary for the silk to adopt fibrillar assemblies, where only globules were observable in nonsheared samples.

DOI: 10.1021/acs.biomac.5b00732
Biomacromolecules 2015, 16, 2796−2804

Transition from Low to High Concentration Regimes of RSF Assembly. In our experiments, RSF exhibited shear-induced self-assembly only at the low concentration of 10 mg/L and not at the much higher concentration of 1000 mg/L. At what concentration does this highly significant change in behavior occur, and why? To address these questions, we sheared RSF at "quasi-logarithmically" increasing intermediate concentrations—20 mg/L, 50 mg/L, 100 mg/L, 200 mg/L, 500 mg/L—and imaged the resulting structures (Figure 2). At concentrations of 10–200 mg/L (Figures 2a–e), the fibrils share a similar morphology as those observed in the 10 mg/L scans: they are short, branched structures. At concentrations of 200 mg/L and below, the protein coat was mostly restricted to the height of a monolayer, i.e. it did not stack, and fibers did not cross each other to form structures more than one layer high. There are areas, however, where protein appears to have accumulated past the single layer in larger globules (insets of Figures 2a,e,f). These globules protrude from clumps of fibrils to heights of 6–7 nm and widths of 60–80 nm, about six times wider and taller than the fibrils (Figure 2g). At a concentration of 500 mg/L (Figure 2f), fibrils are no longer visible, and the surface is completely covered in a globular layer similar to that observed in sheared 1000 mg/L RSF (Figure 1b).

Quantitative Analysis of Low-Concentration Assembly. The low-concentration scans of NSF and RSF displayed distinctive qualitative differences in morphology. We were interested to objectively verify these differences in a quantitative way and thus applied image analysis tools and carried out a rigorous statistical analysis of the results. As schematically shown in Figure 3a, we measured two morphological aspects for each continuous protein assembly: its total footprint area, and branch length of its fibrillar network. These processing procedures were carried out for the AFM data of the 10 mg/L NSF and 10 mg/L, 20 mg/L, 50 mg/L, and 100 mg/L RSF samples. For the higher concentrations of 200 mg/L, 500 mg/L, and 1000 mg/L, the protein formed a fully connected network on the substrate, rendering our procedure ineffective due to the lack of individually assembled structures with finite size.

For the 10 mg/L NSF and RSF samples, our analysis showed that the areas of the assemblies featured highly skewed distributions. These distributions were therefore displayed on a logarithmic scale in Figure 3b (purple axes), in which they interestingly appear relatively symmetric; their medians and first and third quartiles are indicated. NSF particles displayed a median area of 6.50×10^3 nm^2, with a first quartile at 1.56×10^3 nm^2 and third quartile at 19.1×10^3 nm^2; the RSF particles exhibited a median of 1.22×10^3 nm^2, with first and third quartiles at 0.600×10^3 nm^2 and 2.89×10^3 nm^2, respectively. Hence, the assembly sizes were far greater for NSF casts, with a median area ≈5 times larger than median area of RSF casts; the NSF median area was even more than twice as large as the third quartile of RSF assembly areas. To further test the magnitude of the difference between the asymmetric RSF and NSF distributions, two nonparametric measures of effect size were applied. The skew of the sample data and the large difference in sample size (N_{RSF} = 655, N_{NSF} = 51), which is unavoidable due to the nature of the sampling, made a nonparametric measure of effect size preferred over an analytical null hypothesis significance test.[58] The two measurements we employed, Cohen's U_3 and the area under the receiver operating curve (AUROC), both indicate the overlap between two distributions, with a result of 0.5 returned in cases of perfect overlap

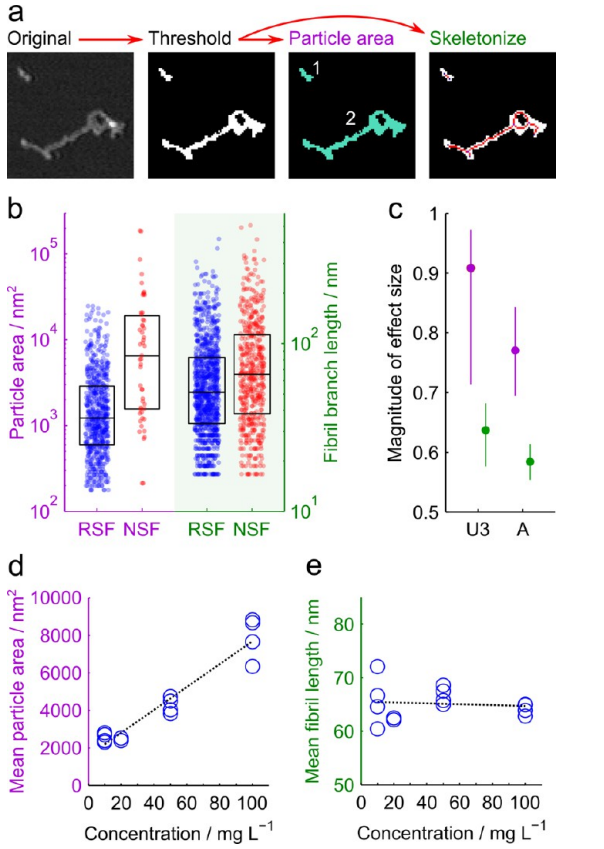

Figure 3. (a) Illustration of our processing procedure. (b) Distributions of continuous particle area (purple axes) and fibril branch length (green axes) for 10 mg/L RSF (blue points) and NSF (red points). The right-skewed data was plotted on a log scale with overlaid boxes to indicate the first quartile, median, and third quartile of data. (c) Effect size measurements and 95% confidence intervals of the difference between RSF and NSF particle area (purple) and fibril branch length (green) as assessed by Cohen's U_3 (U3) and the area under the receiver operating curve (A, see Supporting Information). (d) Mean particle area and (e) mean fibril length observed in scans of RSF assembled structures. The dotted lines represent the first-order lines of best fit to the means.

and a result of 1 indicating minimal overlap (see Supporting Information). Additionally, a result near 1 is strong evidence that the population underlying the second tested distribution (for us, NSF) is greater than the first underlying population (RSF). Our tests returned 95% confidence intervals in the 0.7–0.9 range (Figure 3c, purple bars), suggesting fairly strong support for the conclusion that 10 mg/L NSF assemblies formed under shear possess a greater continuous area than those of RSF.

Fibril length was also tested as another quantitative metric to determine whether one starting product produced longer segments without branching than the other. Skewed distributions were again obtained, but the separation between NSF median branch length (65.7 nm) and that of RSF (51.2 nm) was not nearly as wide as between particle area medians (Figure 3b, green axes). When the same measures of effect size as were applied (see Supporting Information), 95% confidence intervals in the 0.5–0.7 range were returned, indicating a weaker case for longer NSF fibrils (Figure 3c, green bars). These results could indicate either that NSF fibrils are perhaps only slightly longer than RSF fibrils, or that our method of assessing branch length

DOI: 10.1021/acs.biomac.5b00732
Biomacromolecules 2015, 16, 2796–2804

masks the true effect. For instance, a loop in an unbranched fibril would be recognized as three distinct branches by our algorithm.

For RSF, we further analyzed the concentration regime from 10 mg/L−100 mg/L and found that the mean particle areas increased with concentration in an approximately linear fashion (Figure 3d), in parallel with the observed monotonic increase in surface coverage as a function of concentration (Figure S4). This increase in the mean particle area reflects the apparent growth in continuous particles with increasing concentration (compare Figures 2a and 2c), as the mean is more affected by large outliers. No such increase was observed in plots of particle area medians (see Supporting Information, Figure S5) or fibril length means (Figure 3e).

DISCUSSION

Similarities between Native and Reconstituted Silk Fibroin. Based on our analysis of the results, we found similarities as well as differences in the self-assembly of NSF and RSF as a function of concentration and shear (Figure 4). In the absence of shear, we only observed globular features for both NSF and RSF that, by their size and morphology, are likely individual fibroins or clusters thereof (Figures 1e,f, 4a,b). As expected, aerial densities of globules increased with concentration, up to full coverage of the substrate (see Supporting Information, Figure S1). Self-assembly (other than trivial clustering) was not observed in any unsheared NSF or RSF sample of any concentration.

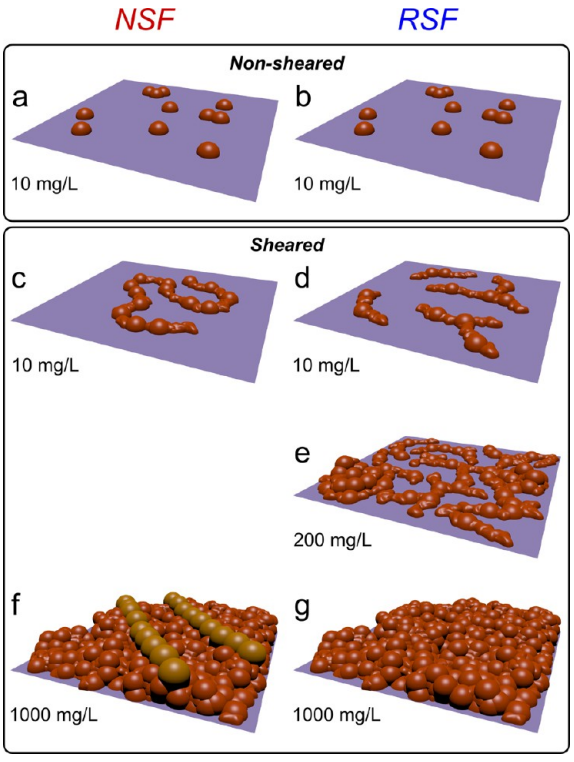

Figure 4. Schematic of NSF and RSF assembly on mica substrate. Nonsheared NSF (a) and RSF (b) formed globules that sporadically aggregated. (c−g) Shearing NSF and RSF triggered protein assembly into fibrils. 10 mg/L NSF (c) assembled into more continuous, coiled fibrils, while 10 mg/L RSF (d) formed shorter, more branched fibrils. While the fibrils mostly occupied a single layer, globular islands pushed past a single layer of coverage at an increased RSF concentration of 200 mg/L (e). At 1000 mg/L, sheared NSF (f) and RSF (g) completely covered the surface in a globular layer, but only in NSF scans were long, beaded fibrils (yellow) observed atop the globules. The apparent differences in NSF and RSF assembly morphology are likely due to disruption of the fibroin molecule during reconstitution.

When sheared, a low 10 mg/L concentration of both RSF and NSF produced fibrils (Figures 4c,d). The fibrils were much larger than the unsheared globules and far too large to represent individual proteins; they are assemblies of several molecules and/or molecular fragments. Other groups have achieved similar fibrillar assembly through heating, treatment with alcohol, electrospinning, simply incubating the solution, or applying cyclical incubation and drying.[34,38−41,43,44,54,57] Our experiments, which were conducted with freshly made fibroin solution in the absence of any other treatment, reflect the importance of shear as a trigger for fibroin self-assembly. We suspect that the sensitivity of fresh fibroin to shear is so high that even samples inadvertently exposed to shear—e.g. by blow-drying, shaking, or vigorous mixing—would undergo self-assembly.[59] This may explain why some studies in the literature report self-assembly in freshly prepared silk samples, even when shearing of samples is not explicitly mentioned.[42,53] Our results, and those of other past studies of NSF[24] and RSF,[40,57] suggest that fibroin forms only a distribution of globules when freshly applied to a mica surface, requiring shear, incubation, or other treatment to assemble into fibrils.

Close inspection of the 10 mg/L RSF and NSF fibrils revealed that both shared a similar substructure: rod-like junctions and disordered regions between globular nodes (Figures 1c,d).[24] These observations suggest that both the RSF and NSF proteins may have been denatured during casting, likely by the combined influences of shear, low concentration, and the substrate surface. This is in line with previous reports that shear partially unfolds the silk molecule, triggering oligomerization with other fibroins,[12] as well as a small angle neutron scattering study demonstrating unfolding of the native silk protein in dilute aqueous solutions.[28] Denaturation due to surface interactions and spin-coating has also been reported for other large amphiphilic molecules.[60−62]

When NSF and RSF were spin-coated at higher concentrations, surface coverage increased, as expected (Figure 4e−g). For RSF, we observed complete coverage for the highest concentrations 500 mg/L and 1000 mg/L (Figures 2f and 1b, respectively). Interestingly, the protein morphology was globular and not fibrillar at these concentrations, which caused us to suspect that the first layer of adsorbed protein may shield subsequently adsorbing proteins from the denaturing influence of the surface. Similarly, sheared NSF exhibited complete coverage with a globular bed of proteins at the highest studied concentration of 1000 mg/L. Although our studies were carried out on mica surfaces, which are distinctly different from the material on the surface of a lubricated silkworm spinning duct,[19,63] one could use our results to speculate about the molecular protein conformation on the surface in vivo. Accordingly, our findings could mean that a first layer of protein covers the spinning duct, avoiding the denaturing of subsequent protein layers. Shearing against this first immobile protein layer, the proteins may then self-assemble into nanofibrils, as was observed in the case of sheared 1000 mg/L NSF, which produced long, straight, beaded protein nanofibrils sitting on top of this globular bed (Figure 1a and 4f). In this hypothetical scenario, the flowing protein would always be in contact with this immobile surface layer of protein. Due to the amphiphilic nature of proteins, they might be

DOI: 10.1021/acs.biomac.5b00732
Biomacromolecules 2015, 16, 2796−2804

capable of forming such a layer on any material, which would have an interesting consequence with respect to the design of future artificial spinning systems: the spinning process would not depend on the material of the spinning duct itself.

Differences between Native and Reconstituted Silk Fibroin. A key outcome of our work is that only the native NSF formed a nanofibrillar structure (Figure 1a) at 1000 mg/L dope concentrations, closely resembling that observed on the surface of native silk fibers.[47−49] This was particularly interesting, since this highest concentration came closest to natural concentrations and was thus arguably the most relevant one. In contrast to NSF, RSF only exhibited randomly distributed, globular protein if prepared under identical concentration and shear conditions (Figure 1b). The loss of native fibrillar morphology in silk assembly observed in RSF would clearly affect the macroscopic material properties. All natural spider and silkworm silks appear to display a nanofibrillar substructure, and there is ample evidence that these fibrils contribute significantly to the prodigious mechanical properties of silks.[64,65] Assembly of RSF into fibrils with native-like structure has been demonstrated;[34,38−41,43,44,54,57] however, while such fibrillar artificial silks are relatively robust compared to other biological materials and promise a novel range of properties in composite applications,[38,44] their mechanical properties still fall short of their natural silk counterparts.[9,38,40,43,44,54,57]

The diminished capability of RSF to self-assemble is in line with past studies that have revealed deviations in the structure and bonding character of the RSF molecule. Gel electrophoresis has shown that reconstitution can fracture the fibroin molecule into 30−200 kDa fragments—far smaller than the native 350 kDa heavy-chain fibroin molecule.[29,66,67] Reconstitution also appears to affect fibroin's bonding character,[6] as a rheological comparison between RSF and NSF revealed vast differences in viscosity response and a stark decrease in the intermolecular association and energy absorption capacity of RSF versus NSF molecules.[26,30]

We find that the "beads-on-a-string" morphology, in which native-like nanofibrils are formed in the 1000 mg/L native fibroin, might point toward an underlying mechanism. One hypothesis is that there are two specific binding sites per fibroin molecule (or per fibroin complex) that bind exactly to two other molecules (or complexes) and thus give rise to the observed linear, "1D" assembly. Potentially related to this phenomenon, recent studies of spider silk protein have revealed that the two highly conserved terminal domains of this protein play a key role in the ordered assembly of a silk fiber.[31,68] While it is as of yet unclear whether these terminal domains similarly facilitate the formation of intermolecular meta-structures in silkworm silk, it has been suggested that the 30 kDa P25 protein associates in storage with the primary components of silkworm fibroin, the 350 kDa heavy chain and 25 kDa light chain, via hydrophobic interaction.[69] Thus, in the same manner that the carboxyl terminal domain of spider silk prealigns the silk molecule for a precise exposure of hydrophobic regions under shear,[14,31] it has been suggested that the alignment of six disulfide-bonded heavy−light chains by a single P25 molecule facilitates the proper folding and assembly of these molecules by interaction of their hydrophobic regions.[69]

RSF does not exhibit the same ordered, 1D assembly as NSF, which could mean in terms of our hypothesis that the reconstitution process yields a significant proportion of fibroin molecules (or complexes) with less than two working binding sites. Accordingly, the highly guided self-assembly that we observed in NSF would be disrupted for RSF. Interestingly, differences we observed in the self-assembly behavior of RSF vs NSF at 10 mg/L are in line with this explanation. First, both dopes formed fibrils under shear, but fibril aggregate sizes and branch lengths were significantly larger for NSF (Figure 3b,c), which further supports our conclusion that the potency for self-assembly is diminished in RSF. Furthermore, RSF fibrils exhibited pronounced branching. The emergence of branching marks a departure from the one-dimensional organization observed in NSF; in our simplified picture, making a branch would require an assembling entity to connect to at least three partners. We hypothesize that when some of the active binding sites and their guiding influence is missing, random assembly takes place, with branching being one of the consequences. Removal of binding sites potentially happens due to the disruptive effect of chaotropic salts on proper terminal domain dimerization, or due to molecular fragmentation—removing enough of the terminal domains altogether. Interestingly, chaotropic agents similar to those used in reconstitution disrupted a crucial salt bridge in the dimeric structure of the carboxyl terminal domain in spider silk, causing the domain to unfold and preemptively expose its hydrophobic regions.[31]

Another, potentially related outcome of our quantitative image analysis is that the distributions of fibril length and particle area were highly skewed for RSF and appeared almost normally distributed when plotted on a log scale. We think that the shape of such distributions may provide insights in the underlying mechanism of self-assembly at these low concentrations. In this particular case, the obtained distribution might be supportive of a nucleation-dependent model of assembly, whereby the rate of fibril growth is proportional to the number of available nucleation sites.[70] This scenario is incompatible with a strictly one-dimensional assembly into linear fibrils, where the number of allowed docking sites per assembly is constant—namely two. Instead, in such an exponential growth-type assembly mode, the growth rate—and thus the number of docking sites for additional protein—would have to be proportional to the aggregate size. This would be fulfilled if branching is allowed. Therefore, the fact that we observe strongly skewed distributions can be interpreted as an additional indicator of disordered and disrupted assembly in RSF.

It is worth noting that the low dope concentration, uncontrolled pH, and salt concentrations in this and many other studies of silk deviate significantly from native in vivo conditions. Regarding concentration, the equilibrium and aggregation behavior of a protein is known to be drastically different in a highly "crowded" or concentrated state,[71,72] and past works showed that fibroin concentration affected several aspects of silk assembly.[30,42] Here it is important to consider that in spin coating, the solvent evaporates until the sample is completely dry, thus continuously increasing the concentration. We only observed the dry end product of this sample preparation procedure, and we do not know at which actual concentration the observed structures were generated, or how close the corresponding conditions were to the in vivo situation. However, since the concentrations in natural silk dope are very high (ca. 24 wt %, about 240,000 mg/L),[15] it is likely that the highest concentration we studied, 1000 mg/L, was closest to natural conditions. To facilitate AFM visualization of molecular-scale features (which tend to be obscured in thicker polymer films), we did not prepare samples from

DOI: 10.1021/acs.biomac.5b00732
Biomacromolecules 2015, 16, 2796−2804

higher solution concentrations. Similarly, our experiments likely also deviated from the complex pH[19,68] and salt[68,73] conditions of in vivo assembly.

Nevertheless, the simple spin-coating routine and imaging by noncontact AFM presented here adds a generic in vitro technique to reveal different regimes of self-assembly as a function of concentration and to test the obtained morphologies for different silk dopes. The quantitative, molecular-scale techniques explored in this work provide a detailed view of morphology at a key level in the hierarchy of silk assembly in response to shear, establishing clear standards of "natural" and "unnatural" assembly. Our approach can be used both for fundamental studies of natural silks and to optimize synthesis and testing of future artificial silk products and assembly procedures. Interesting systems to be tested using our method would be terminal domain-deleted silkworm silk mutants, silkworm silks reconstituted using solvents other than LiBr,[43] and native and recombinant spider silks.[9]

CONCLUSIONS

Our study represents the first molecular-scale comparison of native and reconstituted silkworm protein. In particular, we used AFM to visualize the molecular structures from aqueous NSF and RSF solutions at different concentrations deposited on mica, with and without shear. Several significant qualitative observations were made. First, we found that in the absence of shear, neither NSF nor RSF showed any tendency to self-assemble whatsoever. Instead, we only observed globular protein molecules in varying densities, according to the solution concentrations. Second, we found that at the highest concentration we studied, 1000 mg/L, NSF and RSF exhibited dramatically different behaviors under shear: NSF showed long, straight, nanofibrillar assemblies, closely resembling the structures observed on the surface of natural silk fibers. RSF, in contrast, showed no self-assembly under the same conditions. From this, we concluded that the reconstitution process significantly diminished silk's inherent natural self-assembly capabilities. Furthermore, the quality, consistency, and quantity of our AFM data allowed us to employ quantitative image analysis, which provided us with additional insights. Qualitatively, both NSF and RSF protein solutions at lower concentrations exhibited self-assembly. However, our quantitative analysis of AFM images revealed that NSF assemblies at the same concentration of 10 mg/L were significantly larger than RSF assemblies, further supporting our conclusion of disrupted self-assembly in RSF. Hence, on the basis of our results, we suggest that RSF may not be considered a fully functional silk—both for silk studies and applications. We suggest that an AFM-based morphological characterization of silk assembly, which becomes ever more valuable with the emergence of increasingly powerful quantitative tools,[74] be employed for the comparison of different silks to one another and/or a native standard in future studies of artificial silks.

ASSOCIATED CONTENT

Supporting Information

Contents include an image of unsheared 1000 mg/L NSF, a description of particle area correction factor calculations, scan area consistency evidence, area fraction plots, a description of measures of effect size, and a plot of overlaid mean and median particle areas. The Supporting Information is available free of charge on the ACS Publications website at DOI: 10.1021/acs.biomac.5b00732.

(PDF)

AUTHOR INFORMATION

Present Address

[§]Helmholtz-Zentrum Geesthacht, Zentrum für Material- and Küstenforschung GmbH, Max-Planck-Straße 1, 21502 Geesthacht, Germany.

Funding

This material is based upon work supported by the National Science Foundation under Grant No. DMR-1352542. H.C.S. thanks The Thomas F. and Kate Miller Jeffress Memorial Trust for support under grant number J-1012. F.V. thanks the US Air Force Office of Scientific Research (Grant FA9550-12-1-0294) and the European Research Council (Grant SP2-GA-2008-233409).

Notes

The authors declare no competing financial interest.

REFERENCES

(1) Gosline, J. M.; Guerette, P. A.; Ortlepp, C. S.; Savage, K. N. *J. Exp. Biol.* **1999**, *202*, 3295−3303.
(2) Hakimi, O.; Knight, D. P.; Vollrath, F.; Vadgama, P. *Composites, Part B* **2007**, *38*, 324−337.
(3) Omenetto, F.; Kaplan, D. L. *Science* **2010**, *329*, 528−531.
(4) Kim, D.-H.; Viventi, J.; Amsden, J. J.; Xiao, J.; Vigeland, L.; Kim, Y.-S.; Blanco, J. A.; Panilaitis, B.; Frechette, E. S.; Contreras, D.; Kaplan, D. L.; Omenetto, F. G.; Huang, Y.; Hwang, K.-C.; Zakin, M. R.; Litt, B.; Rogers, J. A. *Nat. Mater.* **2010**, *9*, 511−517.
(5) Kim, T.; McCall, J. G.; Jung, Y. H.; Huang, X.; Siuda, E. R.; Li, Y.; Song, J.; Song, Y. M.; Pao, H. A.; Kim, R.-H.; Lu, C.; Lee, S. D.; Song, I.-S.; Shin, G.; Al-Hasani, R.; Kim, S.; Tan, M. P.; Huang, Y.; Omenetto, F. G.; Rogers, J. A.; Bruchas, M. R. *Science* **2013**, *340*, 211−216.
(6) Vollrath, F.; Porter, D.; Holland, C. *Soft Matter* **2011**, *7*, 9595−9600.
(7) Rising, A.; Widhe, M.; Johansson, J.; Hedhammar, M. *Cell. Mol. Life Sci.* **2011**, *68*, 169−184.
(8) Tao, H.; Kaplan, D. L.; Omenetto, F. G. *Adv. Mater.* **2012**, *24*, 2824−2837.
(9) Rising, A. *Acta Biomater.* **2014**, *10*, 1627−1631.
(10) Vollrath, F.; Knight, D. P. *Nature* **2001**, *410*, 541−548.
(11) Inoue, S.; Tanaka, K.; Arisaka, F.; Kimura, S.; Ohtomo, K.; Mizuno, S. *J. Biol. Chem.* **2000**, *275*, 40517−40528.
(12) Jin, H.-J.; Kaplan, D. L. *Nature* **2003**, *424*, 1057−1061.
(13) Bini, E.; Knight, D. P.; Kaplan, D. L. *J. Mol. Biol.* **2004**, *335*, 27−40.
(14) Eisoldt, L.; Smith, A.; Scheibel, T. *Mater. Today* **2011**, *14*, 80−86.
(15) Laity, P. R.; Gilks, S. E.; Holland, C. *Polymer* **2015**, *67*, 28−39.
(16) Kerkam, K.; Viney, C.; Kaplan, D. L.; Lombardi, S. *Nature* **1991**, *349*, 596−598.
(17) Asakura, T.; Suzuki, Y.; Nakazawa, Y.; Yazawa, K.; Holland, G. P.; Yarger, J. L. *Prog. Nucl. Magn. Reson. Spectrosc.* **2013**, *69*, 23−68.
(18) Suzuki, Y.; Yamazaki, T.; Aoki, A.; Shindo, H.; Asakura, T. *Biomacromolecules* **2014**, *15*, 104−112.
(19) Asakura, T.; Umemura, K.; Nakazawa, Y.; Hirose, H.; Higham, J.; Knight, D. *Biomacromolecules* **2007**, *8*, 175−181.
(20) Holland, C.; Terry, A. E.; Porter, D.; Vollrath, F. *Nat. Mater.* **2006**, *5*, 870−874.
(21) Marsh, R.; Corey, R.; Pauling, L. *Biochim. Biophys. Acta* **1955**, *16*, 1−34.
(22) Kameda, T.; Nakazawa, Y.; Kazuhara, J.; Yamane, T.; Asakura, T. *Biopolymers* **2002**, *64*, 80−85.
(23) Foo, C. W. P.; Bini, E.; Hensman, J.; Knight, D. P.; Lewis, R. V.; Kaplan, D. L. *Appl. Phys. A: Mater. Sci. Process.* **2006**, *82*, 223−233.

DOI: 10.1021/acs.biomac.5b00732
Biomacromolecules 2015, 16, 2796−2804

(24) Greving, I.; Cai, M.; Vollrath, F.; Schniepp, H. C. *Biomacromolecules* **2012**, *13*, 676−682.
(25) Holland, C.; Urbach, J.; Blair, D. *Soft Matter* **2012**, *8*, 2590−2594.
(26) Boulet-Audet, M.; Terry, A. E.; Vollrath, F.; Holland, C. *Acta Biomater.* **2014**, *10*, 776−784.
(27) Rockwood, D. N.; Preda, R. C.; Yucel, T.; Wang, X.; Lovett, M. L.; Kaplan, D. L. *Nat. Protoc.* **2011**, *6*, 1612−1631.
(28) Lee, Y.-W. *Silk Reeling and Testing Manual*, Issue 136; Food & Agriculture Organization of the United Nations: Rome, 1999.
(29) Greving, I.; Dicko, C.; Terry, A.; Callow, P.; Vollrath, F. *Soft Matter* **2010**, *6*, 4389.
(30) Holland, C.; Terry, A.; Porter, D.; Vollrath, F. *Polymer* **2007**, *48*, 3388−3392.
(31) Hagn, F.; Eisoldt, L.; Hardy, J. G.; Vendrely, C.; Coles, M.; Scheibel, T.; Kessler, H. *Nature* **2010**, *465*, 239−242.
(32) Martel, A.; Burghammer, M.; Davies, R. J.; Di Cola, E.; Vendrely, C.; Riekel, C. *J. Am. Chem. Soc.* **2008**, *130*, 17070−17074.
(33) Lefèvre, T.; Rousseau, M.-E.; Pézolet, M. *Biophys. J.* **2007**, *92*, 2885−2895.
(34) Bai, S.; Liu, S.; Zhang, C.; Xu, W.; Lu, Q.; Han, H.; Kaplan, D. L.; Zhu, H. *Acta Biomater.* **2013**, *9*, 7806−7813.
(35) Hansma, H. G.; Kim, K. J.; Laney, D. E.; Garcia, R. A.; Argaman, M.; Allen, M. J.; Parsons, S. M. *J. Struct. Biol.* **1997**, *119*, 99−108.
(36) Oroudjev, E.; Soares, J.; Arcidiacono, S.; Thompson, J. B.; Fossey, S. A.; Hansma, H. G. *Proc. Natl. Acad. Sci. U. S. A.* **2002**, *99*, 6460−6465.
(37) Shulha, H.; Po Foo, C. W.; Kaplan, D. L.; Tsukruk, V. V. *Polymer* **2006**, *47*, 5821−5830.
(38) Ling, S.; Li, C.; Adamcik, J.; Wang, S.; Shao, Z.; Chen, X.; Mezzenga, R. *ACS Macro Lett.* **2014**, *3*, 146−152.
(39) Bai, S.; Zhang, X.; Lu, Q.; Sheng, W.; Liu, L.; Dong, B.; Kaplan, D. L.; Zhu, H. *Biomacromolecules* **2014**, *15*, 3044−3051.
(40) Lu, G.; Liu, S.; Lin, S.; Kaplan, D. L.; Lu, Q. *Colloids Surf., B* **2014**, *120*, 28−37.
(41) Lu, Q.; Wang, X.; Lu, S.; Li, M.; Kaplan, D. L.; Zhu, H. *Biomaterials* **2011**, *32*, 1059−1067.
(42) Lu, Q.; Zhu, H.; Zhang, C.; Zhang, F.; Zhang, B.; Kaplan, D. L. *Biomacromolecules* **2012**, *13*, 826−832.
(43) Zhang, F.; Lu, Q.; Ming, J.; Dou, H.; Liu, Z.; Zuo, B.; Qin, M.; Li, F.; Kaplan, D. L.; Zhang, X. *J. Mater. Chem. B* **2014**, *2*, 3879.
(44) Ling, S.; Li, C.; Adamcik, J.; Shao, Z.; Chen, X.; Mezzenga, R. *Adv. Mater.* **2014**, *26*, 4569−4574.
(45) Terry, A. E.; Knight, D. P.; Porter, D.; Vollrath, F. *Biomacromolecules* **2004**, *5*, 768−772.
(46) Jiang, C.; Wang, X.; Gunawidjaja, R.; Lin, Y.-H.; Gupta, M. K.; Kaplan, D. L.; Naik, R. R.; Tsukruk, V. V. *Adv. Funct. Mater.* **2007**, *17*, 2229−2237.
(47) Du, N.; Yang, Z.; Liu, X. Y.; Li, Y.; Xu, H. Y. *Adv. Funct. Mater.* **2011**, *21*, 772−778.
(48) Poza, P.; Pérez-Rigueiro, J.; Elices, M.; LLorca, J. *Eng. Fract. Mech.* **2002**, *69*, 1035−1048.
(49) Schniepp, H. C.; Koebley, S. R.; Vollrath, F. *Adv. Mater.* **2013**, *25*, 7028−7032.
(50) García, R.; Perez, R. *Surf. Sci. Rep.* **2002**, *47*, 197−301.
(51) Lee, T.; Kashyap, R.; Chu, C. *CVGIP-Graph. Model. Im.* **1994**, *56*, 462−478.
(52) Santos, S.; Barcons, V.; Christenson, H. K.; Font, J.; Thomson, N. H. *PLoS One* **2011**, *6*, e23821.
(53) Inoue, S.; Magoshi, J. U. N.; Tanaka, T.; Magoshi, Y.; Becker, M. *J. Polym. Sci., Part B: Polym. Phys.* **2000**, *38*, 1436−1439.
(54) Zhang, C.; Song, D.; Lu, Q.; Hu, X.; Kaplan, D. L.; Zhu, H. *Biomacromolecules* **2012**, *13*, 2148−2153.
(55) Ma, M.; Zhong, J.; Li, W.; Zhou, J.; Yan, Z.; Ding, J.; He, D. *Soft Matter* **2013**, *9*, 11325.
(56) Fuentes-Perez, M. E.; Dillingham, M. S.; Moreno-Herrero, F. *Methods* **2013**, *60*, 113−121.
(57) Zhang, F.; Zuo, B.; Fan, Z.; Xie, Z.; Lu, Q.; Zhang, X.; Kaplan, D. L. *Biomacromolecules* **2012**, *13*, 798−804.
(58) Hentschke, H.; Stüttgen, M. C. *Eur. J. Neurosci.* **2011**, *34*, 1887−1894.
(59) Shao, Z.; Vollrath, F.; Yang, Y.; Thøgersen, H. C. *Macromolecules* **2003**, *36*, 1157−1161.
(60) Raghavachari, M.; Tsai, H.; Kottke-Marchant, K.; Marchant, R. *Colloids Surf., B* **2000**, *19*, 315−324.
(61) Seyfried, B. K.; Friedbacher, G.; Rottensteiner, H.; Schwarz, H. P.; Ehrlich, H.; Allmaier, G.; Turecek, P. L. *Thromb. Haemostasis* **2010**, *104*, 523−530.
(62) Rabe, M.; Verdes, D.; Seeger, S. *Adv. Colloid Interface Sci.* **2011**, *162*, 87−106.
(63) Renberg, B.; Andersson-Svahn, H.; Hedhammar, M. *Sens. Actuators, B* **2014**, *195*, 404−408.
(64) Nova, A.; Keten, S.; Pugno, N. M.; Redaelli, A.; Buehler, M. J. *Nano Lett.* **2010**, *10*, 2626−2634.
(65) Giesa, T.; Arslan, M.; Pugno, N. M.; Buehler, M. J. *Nano Lett.* **2011**, *11*, 5038−5046.
(66) Um, I. C.; Kweon, H. Y.; Lee, K. G.; Park, Y. H. *Int. J. Biol. Macromol.* **2003**, *33*, 203−213.
(67) Iridag, Y.; Kazanci, M. *J. Appl. Polym. Sci.* **2006**, *100*, 4260−4264.
(68) Andersson, M.; Chen, G.; Otikovs, M.; Landreh, M.; Nordling, K.; Kronqvist, N.; Westermark, P.; Jörnvall, H.; Knight, S.; Ridderstråle, Y.; Holm, L.; Meng, Q.; Jaudzems, K.; Chesler, M.; Johansson, J.; Rising, A. *PLoS Biol.* **2014**, *12*, e1001921.
(69) Tanaka, K.; Inoue, S.; Mizuno, S. *Insect Biochem. Mol. Biol.* **1999**, *29*, 269−276.
(70) Li, G.; Zhou, P.; Shao, Z.; Xie, X.; Chen, X.; Wang, H.; Chunyu, L.; Yu, T. *Eur. J. Biochem.* **2001**, *268*, 6600−6606.
(71) Ellis, R. J. *Trends Biochem. Sci.* **2001**, *26*, 597−604.
(72) Ellis, R. J.; Minton, A. P. *Biol. Chem.* **2006**, *387*, 485−497.
(73) Kronqvist, N.; Otikovs, M.; Chmyrov, V.; Chen, G.; Andersson, M.; Nordling, K.; Landreh, M.; Sarr, M.; Jörnvall, H.; Wennmalm, S.; Widengren, J.; Meng, Q.; Rising, A.; Otzen, D.; Knight, S. D.; Jaudzems, K.; Johansson, J. *Nat. Commun.* **2014**, *5*, 3254.
(74) Usov, I.; Mezzenga, R. *Macromolecules* **2015**, *48*, 1269.

DOI: 10.1021/acs.biomac.5b00732
Biomacromolecules 2015, 16, 2796−2804